



Archived at the Flinders Academic Commons:

<http://dspace.flinders.edu.au/dspace/>

The following article appeared as:

Gascooke, J.R., Alexander, U.N. and Lawrance, W.D., 2012.
Two-dimensional laser induced fluorescence spectroscopy
of van der Waals complexes: fluorobenzene-Ar_n (n=1,2).
Journal of Chemical Physics, 136, 134309.

and may be found at:

http://jcp.aip.org/resource/1/jcpsa6/v136/i13/p134309_s1

DOI: <http://dx.doi.org/10.1063/1.3697474>

Copyright (2012) American Institute of Physics. This article
may be downloaded for personal use only. Any other use
requires prior permission of the authors and the American
Institute of Physics.

Two-dimensional laser induced fluorescence spectroscopy of van der Waals complexes: Fluorobenzene-Arn ($n = 1,2$)

Jason R. Gascooke, Ula N. Alexander, and Warren D. Lawrance

Citation: *J. Chem. Phys.* **136**, 134309 (2012); doi: 10.1063/1.3697474

View online: <http://dx.doi.org/10.1063/1.3697474>

View Table of Contents: <http://jcp.aip.org/resource/1/JCPSA6/v136/i13>

Published by the [American Institute of Physics](#).

Additional information on *J. Chem. Phys.*

Journal Homepage: <http://jcp.aip.org/>

Journal Information: http://jcp.aip.org/about/about_the_journal

Top downloads: http://jcp.aip.org/features/most_downloaded

Information for Authors: <http://jcp.aip.org/authors>

ADVERTISEMENT



Goodfellow
metals • ceramics • polymers • composites
70,000 products
450 different materials
small quantities fast

www.goodfellowusa.com

Two-dimensional laser induced fluorescence spectroscopy of van der Waals complexes: Fluorobenzene-Ar_n (n = 1,2)

Jason R. Gascooke, Ula N. Alexander, and Warren D. Lawrance^{a)}

School of Chemical and Physical Sciences, Flinders University, GPO Box 2100, Adelaide, South Australia 5001, Australia

(Received 27 December 2011; accepted 5 March 2012; published online 3 April 2012)

The technique of two-dimensional laser induced fluorescence (2D-LIF) spectroscopy has been used to observe the van der Waals complexes fluorobenzene-Ar and fluorobenzene-Ar₂ in the region of their S₁-S₀ electronic origins. The 2D-LIF spectral images reveal a number of features assigned to the van der Waals vibrations in S₀ and S₁. An advantage of 2D-LIF spectroscopy is that the LIF spectrum associated with a particular species may be extracted from an image. This is illustrated for fluorobenzene-Ar. The S₁ van der Waals modes observed in this spectrum are consistent with previous observations using mass resolved resonance enhanced multiphoton ionisation techniques. For S₀, the two bending modes previously observed using a Raman technique were observed along with three new levels. These agree exceptionally well with *ab initio* calculations. The Fermi resonance between the stretch and bend overtone has been analysed in both the S₀ and S₁ states, revealing that the coupling is stronger in S₀ than in S₁. For fluorobenzene-Ar₂ the 2D-LIF spectral image reveals the S₀ symmetric stretch van der Waals vibration to be 35.0 cm⁻¹, closely matching the value predicted based on the fluorobenzene-Ar van der Waals stretch frequency. Rotational band contour analysis has been performed on the fluorobenzene-Ar $\bar{0}_0^0$ transition to yield a set of S₁ rotational constants $A' = 0.05871 \pm 0.00014$ cm⁻¹, $B' = 0.03803 \pm 0.00010$ cm⁻¹, and $C' = 0.03103 \pm 0.00003$ cm⁻¹. The rotational constants imply that in the S₁ 0⁰ level the Ar is on average 3.488 Å from the fluorobenzene centre of mass and displaced from it towards the centre of the ring at an angle of ~6° to the normal. The rotational contour for fluorobenzene-Ar₂ was predicted using rotational constants calculated on the basis of the fluorobenzene-Ar geometry and compared with the experimental contour. The comparison is poor which, while due in part to expected saturation effects, suggests the presence of another band lying beneath the contour. © 2012 American Institute of Physics. [<http://dx.doi.org/10.1063/1.3697474>]

I. INTRODUCTION

Van der Waals (vdW) complexes formed between substituted benzenes and argon have become a standard means by which to explore dispersion interactions involving aromatics.¹ Fluorobenzene-Ar (FB-Ar) has received particular attention and has the distinction of being one of the few aromatic systems for which there are high level *ab initio* calculations for both the S₀ and S₁ states,²⁻⁴ motivated by the reasonable set of experimental data available for this species. For each electronic state the calculations provide a number of predictions, including the van der Waals vibrational states in the lower region of the vibrational manifold, the molecular geometry and the binding energy. Currently, experimental data are available concerning the S₀ and S₁ binding energies,^{5,6} the S₀ rotational constants,^{7,8} and hence S₀ geometry, and a number of the S₁ van der Waals vibrational levels.^{5,6,9-11} However, the S₁ rotational constants, and hence the S₁ geometry for the complex, have yet to be satisfactorily determined⁴ and, with the exception of the two bend fundamentals,¹² the S₀ van der Waals vibrational level structure remains unobserved. The sit-

uation for FB-Ar, where there are few reports of the van der Waals vibrational levels associated with the ground state, is typical of that for van der Waals complexes more generally. A significant contributor to this paucity of data is the lack of straightforward experimental techniques with sufficient sensitivity.

We have recently reported a two dimensional laser induced fluorescence (2D-LIF) technique¹³ for teasing apart the rotational contours of polyatomic molecules at room temperature, and hence determining accurate rotational constants. As a demonstration of the technique's sensitivity, we reported spectral features associated with ¹³C and ²H isotopomers of fluorobenzene (FB) in natural abundance in a supersonic free jet expansion. The high sensitivity coupled with an ability to distinguish different species in the expansion suggest that the technique will be useful for observing and separating weak features associated with a specific van der Waals complex.

The present work illustrates the power of 2D-LIF spectroscopy for probing fluorescing van der Waals molecules in their S₀ and S₁ states. Specifically, we show that it is able to address the shortcomings identified above in the experimental data set for FB-Ar, allowing a more rigorous test of the *ab initio* predictions than has been possible to date. The images produced in 2D-LIF spectroscopy are shown to provide

^{a)} Author to whom correspondence should be addressed: Electronic mail: warren.lawrance@flinders.edu.au.

a means for detecting specific complexes in the supersonic expansion with reduced spectral overlap.¹³

In addition to its application to FB-Ar, we have used 2D-LIF spectroscopy to explore the FB-Ar₂ (1|1) van der Waals trimer. (The nomenclature (1|1) indicates that there is one Ar atom attached to each face of the aromatic ring.) Little has been reported concerning this complex; however, from an analysis of the FB-Ar 2D-LIF spectral images a number of observables for FB-Ar₂ (1|1) can be predicted, including the rotational constants and vibrational frequencies. In aromatic-Ar₂ (1|1) complexes, the interaction between the two Ar atoms is negligible and there is essentially no alteration in the strength of the aromatic-Ar interaction.^{14–19} Consequently, the Ar position in the aromatic-Ar is duplicated for the aromatic-Ar₂ system and relationships between various observables, such as the vibrational frequencies, can be derived.^{9,12} These relationships can aid assignments in the dimer and trimer complexes.

The FB-Ar complex has been studied for many years. The ground state geometry of the complex has been inferred from the known FB geometry and the FB-Ar rotational constants determined using microwave studies.^{7,8} Two structures satisfy the rotational constants. These differ in the direction of displacement of the Ar atom from the FB centre of mass (CoM), with Ar being either towards the C–F bond or towards the centre of the ring. A study using isotopically substituted samples has shown that the correct structure has the Ar displaced towards the centre of the ring and away from the C–F bond.⁸ Vibrational frequencies of the two van der Waals bending vibrations in S₀ have been determined using stimulated Raman spectroscopy.¹²

Regarding the S₁ state of the FB-Ar complex, as is usual with aromatic-rare gas complexes the dispersion interaction is stronger in the excited electronic state, resulting in the S₁-S₀ origin transition being red shifted by 24 cm⁻¹ compared with the monomer.^{5,6,9–11,20,21} Several S₁ van der Waals vibrations have been observed in the S₁ ← S₀ excitation spectrum. An early study by Bieske *et al.* introduced a stretch-bend anharmonic coupling scheme to explain the intensities and band positions observed,⁹ but the application of this scheme was subsequently shown to be in error since they had mistakenly assigned a bend fundamental to an overtone.² Nevertheless, the proposal that there is coupling between the stretch and the bend overtone has merit and is explored in this work. Ford and Müller-Dethlefs determined a set of S₁ rotational constants as part of their zero kinetic energy (ZEKE) study of the complex and its cation.²² Interestingly, subsequent *ab initio* calculations have questioned the accuracy of these constants given the large difference between the observed and computed values.⁴ Lembach and Brutschy studied the neutral and cation spectra using mass analysed threshold ionisation and were able to determine an upper limit for the dissociation energy of the complex: $D_0 = 344 \text{ cm}^{-1}$ in S₀.^{5,10} They also reported a study of dissociation in the larger complexes, FB-Ar₂ and FB-Ar₃. An earlier study by Rademann *et al.* reported resonance enhanced multiphoton ionisation (REMPI) spectra of FB-Ar_{1–5} and FB_{1–3} clusters.²³ These are the only studies that we are aware of for these larger complexes.

Ab initio calculations of the FB-Ar complex in the ground electronic state were first reported by Hobza *et al.* in 1993.²⁴ These authors used a MP2 level approach with a 6-31+G* basis set for the FB π system and [7s4p2d] basis set for Ar. Subsequently, in 2001 Tarakeshwar *et al.* undertook more extensive calculations, also at the MP2 level, using a larger basis set, accounting for basis set superposition error, and including zero point energy to determine the ground state binding energy.²⁵ In 2004 Fajín *et al.* reported calculations of the ground state potential energy surface, including the van der Waals vibrational levels up to 75 cm⁻¹, using the coupled-cluster singles and doubles including connected triple excitations (CCSD(T)) model.² The subsequent study by Makarewicz, using a MP2 approach, reported vibrational levels up to 70 cm⁻¹.³ Due to the lack of experimental data, the authors of both studies largely compared their S₀ frequencies with observed S₁ frequencies (the exception being the two bend fundamentals observed using Raman spectroscopy¹²). Fajín *et al.* noted that the availability of theoretical values could aid future assignments as experimental data became available. Fajín *et al.* subsequently extended their work to the S₁ surface, again calculating the vibrational level structure in the lower part of the intermolecular potential.⁴ Their predicted S₁ rotational constants differ significantly from those determined from the experimental contour recorded by Ford and Müller-Dethlefs,²² particularly the C constant which the authors suggest is too large.

There has been little reported concerning the FB-Ar₂ complex. The S₁-S₀ spectral shift has been reported as -47 cm⁻¹ (Refs. 10, 11, 20, and 21) and -50 cm⁻¹ (Ref. 9), essentially twice the FB-Ar shift, confirming that the complex is the (1|1) species. No intermolecular vibrational frequencies or rotational constants have been reported for S₁ or S₀.

In order to expand the range of experimental observables for the FB-Ar_{1,2} complexes, we have applied the sensitive technique of 2D-LIF spectroscopy to observe the vibrational frequencies of a number of van der Waals vibrations of FB-Ar in the ground electronic state, allowing comparison with *ab initio* calculations. Furthermore, we were able to observe the FB-Ar₂ van der Waals symmetric stretch vibration. Finally, to resolve the differences between the rotational constants determined from experiment and *ab initio* calculations for FB-Ar, a band contour analysis of the rotational contour observed in the 2D-LIF images was undertaken to determine the S₁ rotational constants afresh, and hence obtain a revised set of structural parameters for this complex.

II. EXPERIMENTAL DETAILS

The experimental setup for our 2D-LIF has been given in detail in a previous publication.¹³ The salient features for the present experiments are as follows. The frequency doubled output of a Nd:YAG pumped dye laser (Continuum Surelite-II pumping a Lambda Physik Scanmate operating with coumarin 503 laser dye; 0.3 cm⁻¹ doubled line width; 10 Hz repetition rate) is passed vertically through a stainless steel chamber containing the source, the vertical propagation matching the vertical entrance slit of the spectrometer. The laser beam intersects a horizontal supersonic free jet

expansion of 1% FB in Ar at $X/D \sim 10$. The resulting fluorescence is dispersed using a home-built spectrometer with a dispersion of $\sim 5 \text{ cm}^{-1}$ per mm in the wavelength region of the present experiments. The dispersed fluorescence is detected with a 25 mm diameter gated image intensifier with single photon detection sensitivity. The loss of sensitivity at the edges (due to the image intensifier vertical dimension no longer matching the slit height) leads to the effective width of the region viewed being $\sim 80\text{--}100 \text{ cm}^{-1}$. The image intensifier is gated to detect fluorescence in a time window near the laser; for the experiments described herein, it was gated to open post the laser pulse to minimise the detection of scattered laser light. The image intensifier output at each laser shot is captured using a charge coupled device (CCD) camera. The CCD image is downloaded to a computer and analysed to identify and record the centre of each spot observed and a histogram of events at each camera pixel position is built up. The process continues for a preset number of laser shots with the laser fixed in wavelength, producing a section of the dispersed fluorescence spectrum at that laser wavelength. The laser then steps to the next wavelength and the process repeats until the laser has scanned the region required. The result is a three-dimensional surface of fluorescence intensity as a function of both the laser and dispersed fluorescence wavelengths. We refer to this surface as a 2D-LIF spectral image.

III. RESULTS

A. Background: Features expected in the 2D-LIF spectral images

Before presenting the data we discuss the type of information that the 2D-LIF spectral images provide. The supersonic expansion contains a variety of species FB_nAr_m , where n and m range independently from zero upwards in integer steps. Since we probe in the region of the FB S_1 - S_0 origin transition, the experiment is blind to Ar_m clusters. The dominant species observed in the experiment is uncomplexed FB. The FB-Ar and FB-Ar₂ (1|1) complexes of interest have been observed previously using REMPI in conjunction with time of flight mass spectrometry so their origin transitions are known, as are several transitions involving the van der Waals modes for FB-Ar.^{5,6,9-11,20,21} FB-Ar₃ has been observed and its origin reported to be blue shifted 4.8 cm^{-1} (Ref. 23) and 6.5 cm^{-1} (Ref. 10) from the FB origin. Larger FB-Ar_n clusters show multiple peaks both red and blue shifted,²³ but are unlikely to be seen under our expansion conditions. The REMPI spectrum of homogenous clusters, FB_n , shows a very broad absorption feature centred around the FB origin that is several hundred wavenumbers wide and has sharp features sitting on top. Thus we expect a 2D-LIF scan in the region of the FB origin band to reveal transitions associated with FB, FB-Ar, FB-Ar₂, and possibly FB-Ar₃ depending on the sensitivity. The rotational constants are anticipated to be different for these species and consequently the shapes of the rotational structure associated with each in the 2D-LIF images will also differ and provide a signature for each species.

The images are presented with the laser wavenumber along the x axis and the fluorescence wavenumber along the

axis, unless specified otherwise. Where the dispersed fluorescence monitors the origin band region and the laser scans the same region, the origin bands for the various species appear along the image diagonal running from the bottom left to top right, i.e., the line corresponding to the same absorption and emission wavenumbers. In the case of the complexes, where a transition leads to excitation of a van der Waals vibration in S_1 the image is expected to show a feature nearly horizontal with the complex's origin transition. The reason for this is as follows. The absorption to S_1 occurs via a transition of the form νdW_n^0 , where νdW indicates a van der Waals vibration. The van der Waals modes are calculated to have similar frequencies in the two electronic states.²⁻⁴ Because of the similarity of these modes in S_0 and S_1 , the Franck Condon factors are expected to lead to the primary emission being via a $\Delta v = 0$ transition, i.e., νdW_n^0 , which has close to the same wavenumber value as the origin transition. Thus the most intense van der Waals transitions are vertically displaced below the image diagonal by the ground state frequency of νdW_n . For this reason, excitation to a number of S_1 van der Waals vibrations of the same species leads to a series of transitions that will appear at a similar emission wavenumber but different absorption wavenumbers. Where the fluorescence spectrum reveals S_0 van der Waals vibrations, they appear as bands displaced vertically from the image diagonal. The images can thus reveal both the S_0 and S_1 van der Waals mode frequencies. While 2D-LIF is not a mass selective technique, the different spectral signatures of the various species in the expansion allow, within limits, features in the image to be associated with particular complexes.

B. Overview of the 2D-LIF spectral images of FB-Ar₀₋₂

Figure 1(a) shows a survey 2D-LIF image of FB cooled in a supersonic free jet expansion of argon, recorded in the region around the origin band at $37\,813.8 \text{ cm}^{-1}$. The FB features seen in this image have been discussed previously.¹³ The intense feature at $(37\,813.8 \text{ cm}^{-1}, 37\,813.8 \text{ cm}^{-1})$ is the origin band of fluorobenzene and the shape of this band provides a fingerprint for fluorobenzene bands. The nomenclature (x,y) introduced here refers to an (excitation, emission) position on the image. Thus the 30_1^1 sequence band²⁶ at $(37\,797.1 \text{ cm}^{-1}, 37\,797.1 \text{ cm}^{-1})$ is easily identified as belonging to fluorobenzene because of the image shape, as is the ^{13}C band shifted 4.0 cm^{-1} to higher energy from the origin band.¹³ The presence of the sequence band indicates incomplete vibrational cooling in the free jet expansion.

Fluorobenzene-Ar is reported to absorb 24 cm^{-1} red shifted from the fluorobenzene transitions.^{5,6,9-11,20,21} The band at $(37\,790.7 \text{ cm}^{-1}, 37\,790.7 \text{ cm}^{-1})$ is thus identified as the fluorobenzene-Ar 0_0^0 transition. It is clear that the shape of this band is distinctly different from the fluorobenzene bands, showing an intense Q branch feature. This assignment gives a red shift for the complex of 23.1 cm^{-1} , slightly lower than the values reported previously. This is almost certainly due to previous groups reporting the shift from the maximum of the FB contour, whereas the resolution of our excitation source allows us to report origin values for the band. The rotational

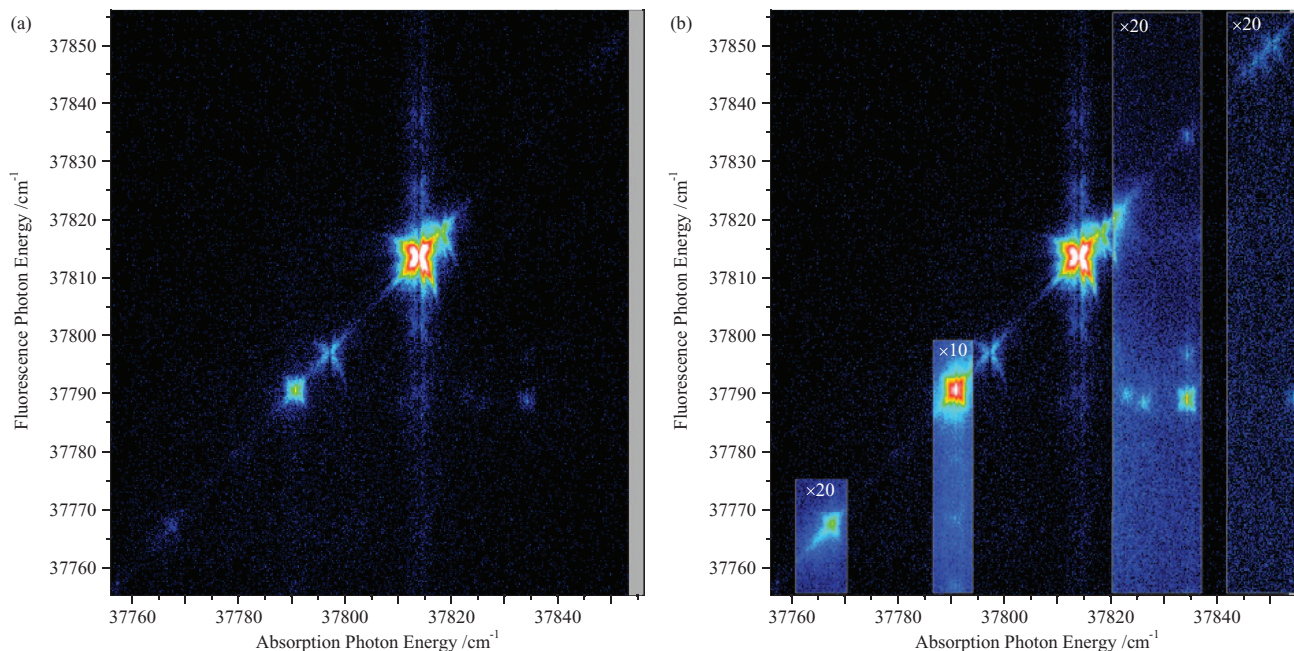


FIG. 1. (a) A two-dimensional laser induced fluorescence (2D-LIF) image of a supersonic free jet expansion of fluorobenzene (FB) in argon in the region of the FB 0_0^0 transition. The laser wavenumber is along the horizontal axis, while the dispersed fluorescence wavenumber is along the vertical axis. The image shows features due to FB, FB-Ar, and FB-Ar₂. The features above and below the intense FB feature at an absorption photon energy of 37 813.8 cm⁻¹ are grating ghosts. (b) The image shown in (a) with enhanced 2D-LIF scans of key regions inserted to better reveal weaker features of the image. The intensities of the inserted sections are increased by the factor indicated on the enhanced section.

origin for FB is known to occur at the minimum of the contour.¹³ Our reported values for FB refer to the minimum of the FB contour, whereas FB-Ar values are reported for the peak of the Q branch.

The FB-Ar rotational structure is replicated in several bands below the image diagonal, indicating that they are associated with this complex. These bands are a consequence of absorption to S_1 van der Waals modes of the form vdW_n^0 . As discussed above, the most intense fluorescence transitions associated with these absorption bands are of the form vdW_n^n , which are displaced vertically below the image diagonal by the ground state frequency of vdW_n . The Franck-Condon factors strongly favour $\Delta v = 0$ transitions in the van der Waals modes and as a result the diagonal features, which arise from the same $\Delta v = 1$ or 2 change in both absorption and emission, are very weak compared with the off-diagonal $\Delta v = 0$ emission.

Images were obtained with improved signal in key regions associated with absorption by the van der Waals complexes and sections of these are shown in Fig. 1(b). These additional images enable the van der Waals modes in particular to be identified. The transitions observed in the images are summarised in Table I. The majority are associated with the FB-Ar van der Waals complex. Those associated with FB have been discussed above, with the exception of the weak features in the top right hand corner of Fig. 1(b), which are due to mono-deuterated FB in natural abundance.^{13,26–28} Where transitions associated with the van der Waals species have been reported previously, these values are included in the table. The S_1 van der Waals vibrations seen in the image have been reported previously. The two S_0 bend fundamentals have been reported previously¹² to be at 22.5 cm⁻¹ and

33.5 cm⁻¹ and there are very weak features discernible in the appropriate regions of the image in Fig. 1(b). The S_0 van der Waals frequencies and features are discussed in more detail in Sec. III D.

The 0_0^0 transition of the FB-Ar₂ (1|1) conformer has been reported previously to have a red shift of 46 cm⁻¹ from the FB 0_0^0 band^{10,11,20,21} and a transition is observed in the 2D-LIF image where expected on the diagonal at 37 767.4 cm⁻¹ and 37 767.4 cm⁻¹. It is clearly identified as a separate species by the rotational pattern. The origin band of FB-Ar₃ is not seen due to overlap with the strong FB ¹³C origin band feature.

C. LIF spectrum of FB-Ar: S_1 van der Waals features

Vertical slices extracted from the image and integrated horizontally give the fluorescence spectrum for the range of laser wavenumbers included in the slice. Horizontal slices integrated vertically give the LIF spectrum generated by those species that fluoresce in the region covered by the height of the slice. By varying the position and height of the slice, one can extract the LIF spectrum for a particular species (or several species), with the 2D-LIF spectral image showing the extent to which the chosen slice contains contributions from more than one species. Effectively, this is the equivalent of viewing the LIF spectrum using a variable narrow bandpass filter that can be tuned post the experiment. To illustrate this, Fig. 2 shows the LIF spectrum for FB-Ar, including the van der Waals vibrations, extracted from a horizontal slice of Fig. 1 chosen to include the FB-Ar vdW_n^n transitions. This largely

TABLE I. A summary of the transitions associated with FB, FB-Ar, and FB-Ar₂ observed in the 2D-LIF images.

Species ^a	Position (absorption /cm ⁻¹ , fluorescence /cm ⁻¹)	Intensity	Assignment (absorption, fluorescence)	Absorption shift ^b (cm ⁻¹)	Fluorescence displacement ^c (cm ⁻¹)
FB	(37813.8, 37813.8)	10 000	(0 ₀ ⁰ , 0 ₀ ⁰)	0	0
	(37797.1, 37797.1)	147	(30 ₀ ¹ , 30 ₁ ¹)	-16.7	0
FB-Ar (-23.1 cm ⁻¹) ^d	(37790.7, 37790.7)	295	(0 ₀ ⁰ , 0 ₀ ⁰)	0	0
	(37790.7, 37768.4)	2.0	(0 ₀ ⁰ , b1 ₁ ⁰)	0	-22.3 ^e
	(37790.7, 37756.9)	2.0	(0 ₀ ⁰ , bs ₁ ⁰)	0	-33.8 ^f
	(37790.7, 37753.1)	4.6	(0 ₀ ⁰ , bl ₂ ⁰)	0	-37.6
	(37790.7, 37745.3)	6.7	(0 ₀ ⁰ , s ₁ ⁰)	0	-45.4
	(37810.5, 37788.3)	1.3	(b1 ₀ ¹ , b1 ₁ ¹)	19.7 ^g	-22.2 ^e
	(37822.9, 37789.5)	3.8	(bs ₀ ¹ , bs ₁ ¹)	32.2 ^h	-33.4 ^f
	(37826.1, 37788.5)	3.7	(bl ₀ ² , bl ₂ ²)	35.3 ⁱ	-37.6
	(37826.1, 37780.7)	0.2	(bl ₀ ² , bl ₀ ² s ₁ ⁰)	35.3 ⁱ	-45.3
	(37834.2, 37834.2)	1.0	(s ₀ ¹ , s ₀ ¹)	43.5 ^j	0
	(37834.2, 37796.6)	1.0	(s ₀ ¹ , s ₀ ¹ bl ₂ ⁰)	43.5 ^j	-37.6
	(37834.2, 37788.9)	14	(s ₀ ¹ , s ₁ ¹)	43.5 ^j	-45.4
	(37854.3, 37789.2)	1.8	(bs ₀ ² , bs ₂ ²)	63.5 ^k	-65.0
FB-Ar ₂ (-46.4 cm ⁻¹) ^l	(37767.4, 37767.4)	24	(0 ₀ ⁰ , 0 ₀ ⁰)	0	0
	(37767.4, 37732.4)	1.5	(0 ₀ ⁰ , s1 ₁ ⁰)	0	-35.0

^aObserved shift from the fluorobenzene 0₀⁰ transition is given in parentheses.

^bObserved shift from the 0₀⁰ absorption of the relevant species FB, FB-Ar, or FB-Ar₂.

^cObserved shift from the excitation wavenumber determined as (fluorescence wavenumber - excitation wavenumber). A value of zero indicates that the transition appears on the image diagonal. A negative value indicates that fluorescence is occurring to a vibrational level above the initial level from which excitation occurred; in this case the energy of the terminating level is above the energy of the initial level by the absolute value of the observed shift.

^dReported shift from FB 0₀⁰ absorption transition: -23 cm⁻¹ (Ref. 23), -24 cm⁻¹ (Refs. 5, 6, 9-11, 20, and 21).

^eReported ground state frequency of b1₁: 22.5 cm⁻¹ (Ref. 12).

^fReported ground state frequency of bs₁: 33.5 cm⁻¹ (Ref. 12).

^gReported shifts from FB-Ar 0₀⁰ absorption transition: 17 cm⁻¹ (Ref. 11), 20 cm⁻¹ (Refs. 6 and 10), 21 cm⁻¹ (Ref. 9).

^hReported shifts from FB-Ar 0₀⁰ absorption transition: 32 cm⁻¹ (Refs. 6, 10, and 11), 34 cm⁻¹ (Ref. 9).

ⁱReported shifts from FB-Ar 0₀⁰ absorption transition: 35 cm⁻¹ (Refs. 6 and 11), 38 cm⁻¹ (Ref. 9).

^jReported shifts from FB-Ar 0₀⁰ absorption transition: 43 cm⁻¹ (Refs. 5, 11, and 23), 43.5 cm⁻¹ (Ref. 10), 44 cm⁻¹ (Ref. 6), 47 cm⁻¹ (Ref. 9).

^kReported shifts from FB-Ar 0₀⁰ absorption transition: 64 cm⁻¹ (Ref. 6), 70 cm⁻¹ (Ref. 9).

^lReported shifts from FB 0₀⁰ absorption transition: -46 cm⁻¹ (Ref. 23), -47 cm⁻¹ (Refs. 10, 11, 20, and 21), -50 cm⁻¹ (Ref. 9).

eliminates the FB transitions in the same way that mass selective REMPI spectra allows for observation of a single species. One does need to be aware that limiting the fluorescence bands observed can affect the relative intensity of bands in the LIF spectrum. In the present case, we observe features arising from absorption via vdW_0^n and emission via vdW_n^n . To a first approximation vdW_n^n emission transitions have the same Franck Condon factor and so the spectrum provides a measure of the relative vdW_0^n intensities.

In order of increasing wavenumber, the features seen correspond to the 0₀⁰ band (0 cm⁻¹), the long axis bend, b1₀¹ (+19.7 cm⁻¹), the short axis bend, bs₀¹ (+32.2 cm⁻¹), the first overtone of the long axis bend, bl₀² (+35.3 cm⁻¹), the stretch, s₀¹ (+43.5 cm⁻¹), and the first overtone of the short axis bend, bs₀² (+63.5 cm⁻¹). These values closely match those reported

previously, as shown in Table I. It should be noted that the long axis bend fundamental is partly obscured by grating ghosts associated with the strong FB origin band but can be made out by careful examination of the 2D-LIF image.

D. Dispersed fluorescence spectrum of FB-Ar: S₀ van der Waals features

As noted above, for S₀ only the two bend fundamentals have been previously reported. In order to probe for the S₀ van der Waals frequencies, we have scanned a small region of the LIF spectrum while monitoring the low displacement region where the van der Waals modes are expected to be observed in dispersed fluorescence. Figure 3 shows the image of the region scanned and the dispersed fluorescence spectrum extracted. Note that since the focus is on the dispersed fluorescence spectrum in order to view S₀ modes, this image is

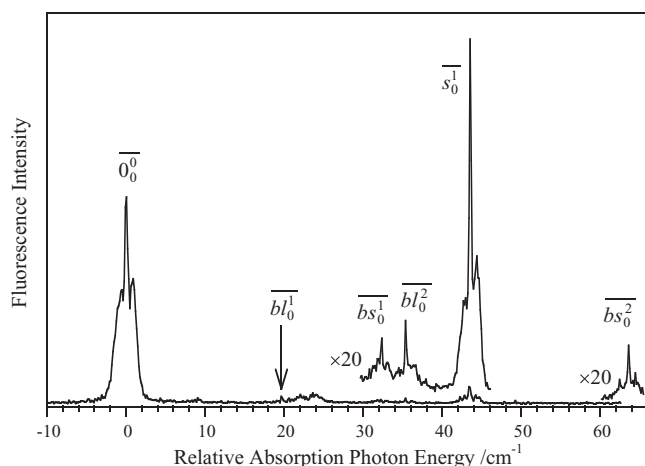


FIG. 2. The LIF spectrum of FB-Ar extracted by vertically integrating a horizontal slice taken from Fig. 1. The slice encompasses FB-Ar van der Waals bands while minimising contributions from other species. The lower trace is from Fig. 1(a), while the $\times 20$ spectra are generated from the enhanced 2D-LIF segments in Fig. 1(b). The feature between $+21$ and $+25$ cm^{-1} is due to a grating ghost associated with the origin band of FB.

different to those shown in Fig. 1 as it has the laser wavenumber varying along the vertical axis and the dispersed fluorescence along the horizontal axis. The image is integrated along the laser axis to reveal the FB-Ar $\overline{0_0^0}$ dispersed fluorescence spectrum. The van der Waals fundamentals observed are the long axis bend at 22.2 cm^{-1} , the short axis bend at 33.4 cm^{-1} , and the stretch at 45.4 cm^{-1} . The long axis bend overtone is observed at 37.6 cm^{-1} . From Fig. 1(b), the two quantum level of the short axis bend is at 65.0 cm^{-1} . The only previous report of S_0 frequencies for the FB-Ar complex comes from Maxton *et al.* who used a Raman technique to reveal the long and short axis bend fundamentals, $\nu_{bl} = 22.5$ cm^{-1} and $\nu_{bs} = 33.5$ cm^{-1} , respectively.¹² Our values are consistent

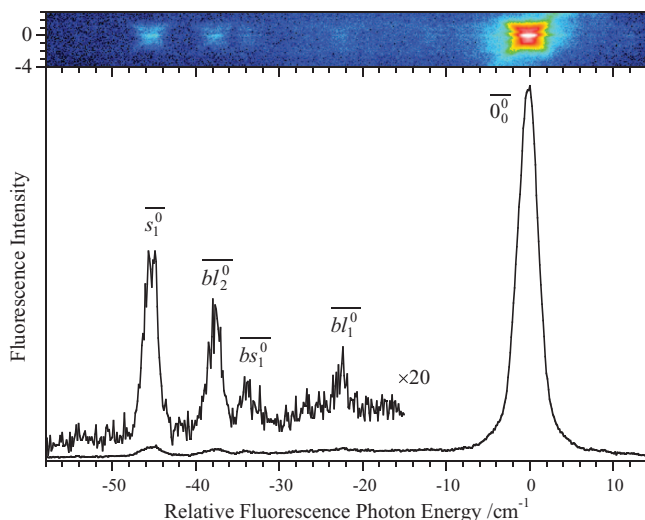


FIG. 3. The 2D-LIF image and corresponding dispersed fluorescence spectrum arising from scanning the laser over the $\overline{0_0^0}$ band of FB-Ar and monitoring dispersed fluorescence in the region near $\overline{0_0^0}$. Because the dispersed fluorescence spectrum is the focus here, the image is displayed with the laser wavenumber on the vertical axis and dispersed fluorescence wavenumber along the horizontal axis. The dispersed fluorescence spectrum is extracted by integrating the image along the laser wavenumber axis.

with these. Confirmation of the S_0 and S_1 assignments comes from the Franck Condon factors observed in the image seen in Fig. 1(b). The most intense emission from an S_1 van der Waals level terminates in the corresponding S_0 level, identifying the S_0 frequency for that state.

The images provide the first measurements of the stretch fundamental and the long and short axis bend overtones in S_0 . The S_1 van der Waals fundamentals are between 1.2 and 2.5 cm^{-1} lower in frequency than the corresponding S_0 values. In S_0 the long axis bend overtone occurs well below twice the fundamental frequency, suggesting significant diagonal anharmonicity for this mode or that it is affected by a Fermi resonance with the stretch as suggested by Bieske *et al.* for the S_1 state.⁹ This will be discussed in detail in Sec. IV C.

E. FB-Ar rotational contour and rotational constants

The FB-Ar $\overline{0_0^0}$ band has a sharp, strong, central Q branch, indicative of a parallel band. The LIF $\overline{0_0^0}$ rotational contour was recorded by scanning the laser while integrating only the $\overline{0_0^0}$ fluorescence transition. The power dependence of the signal was measured and was found to be linear up to $\sim 3 \times 10^3$ Wcm^{-2} . To ensure that the observed rotational contour was not subject to saturation effects, a laser power of 2.5×10^3 Wcm^{-2} was employed. The resulting LIF spectrum is shown in Fig. 4. By comparing this LIF spectrum with that obtained from the extended scan (see Fig. 2), the effects of saturation are clear. Saturation leads to reduced intensity of the Q branch relative to the peaks of the P and R branches. Interestingly, of the previously published spectra only the ZEKE spectrum reported by Ford and Müller-Dethlefs does show Q branch structure similar to that seen in our spectrum.²² However, the relative intensity of the features suggests that there remains a residual influence of saturation effects in their spectrum. All other published spectra have not revealed the

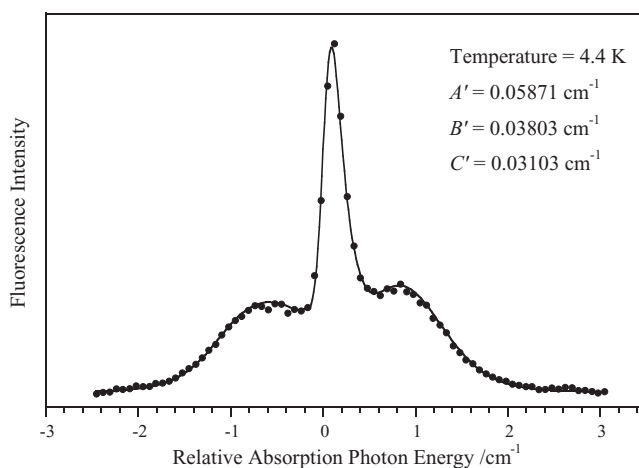


FIG. 4. The LIF contour for the FB-Ar $\overline{0_0^0}$ band extracted by integrating only the $\overline{0_0^0}$ fluorescence band. A low laser fluence (known to be in the linear absorption regime) was used to eliminate saturation effects. The best-fit contour and rotational constants are also shown (see text). The x axis represents displacement from the band origin. The band maximum is shifted approximately $+0.1$ cm^{-1} . All rotational constants associated with the fit are given in Table II.

TABLE II. FB-Ar $\overline{0}_0^0$ rotational constants determined from experimental and *ab initio* studies. The previously reported values are provided for comparison. The S_0 values, needed to calculate the 0_0^0 rotational contour, are also given.

Constant (cm^{-1})	S_0		S_1	
	Stahl and Grabow ^a	This work ^b	Ford and Müller-Dethlefs ^c	Fajín <i>et al.</i> ^d
A	0.060435599	0.05871 ± 0.00014	0.059151	0.05841
B	0.036863157	0.03803 ± 0.00010	0.038323	0.03713
C	0.030082238	0.03103 ± 0.00003	0.033251	0.03032
Δ_J	8.968×10^{-8}			
Δ_{JK}	2.794×10^{-7}			
Δ_K	-2.761×10^{-7}			
δ_J	2.201×10^{-8}			
δ_K	2.006×10^{-7}			

^aReference 7.

^bDetermined by fitting the $\overline{0}_0^0$ rotational contour shown in Fig. 4.

^cExperimental, Ref. 22.

^d*Ab initio*, Ref. 4.

rotational detail seen in this contour,^{5,6,9–11} possibly because of a combination of lower resolution excitation sources being used and saturation effects distorting the rotational contour.

The contour was fitted to extract rotational constants for the S_1 state of the FB-Ar complex; the resulting fit is also shown in Fig. 4. The rotational constants for the S_0 state were taken from the microwave study by Stahl and Grabow⁷ with the higher order terms (centrifugal constants) being retained for the S_1 state. The rotational constants determined for the S_1 state are listed in Table II. The fitting procedure used the asymmetric rotor program of Western²⁹ to calculate the rotational energies and transition intensities. Because the contour is not replete with features at our experimental resolution, this program was incorporated within two separate programs to explore the uniqueness of the constants determined. The first utilized a Monte Carlo approach whereby random sets of rotational constants were chosen to explore the fitting surface, with their “quality” expressed in terms of the sum of the squares of the differences between the observed and calculated contours. This process explored a large range of possible constants and identified the set that minimised this difference. Second, a nonlinear least squares fitting program was used to determine the best-fit constants. Both methods identified the same set of constants within the uncertainties quoted, leading us to be confident in the values reported. The quoted uncertainties represent one standard deviation as determined by the least squares fitting algorithm.

F. Dispersed fluorescence spectrum of FB-Ar₂: S_0 van der Waals features

No van der Waals vibrational frequencies have been reported for FB-Ar₂. Analogous to the case for FB-Ar described in Sec. III D, to probe for the S_0 van der Waals frequencies of this complex we have scanned a small region of the LIF spectrum while monitoring the low displacement region in dispersed fluorescence where the van der Waals modes are expected. Figure 5 shows the image of the region scanned and

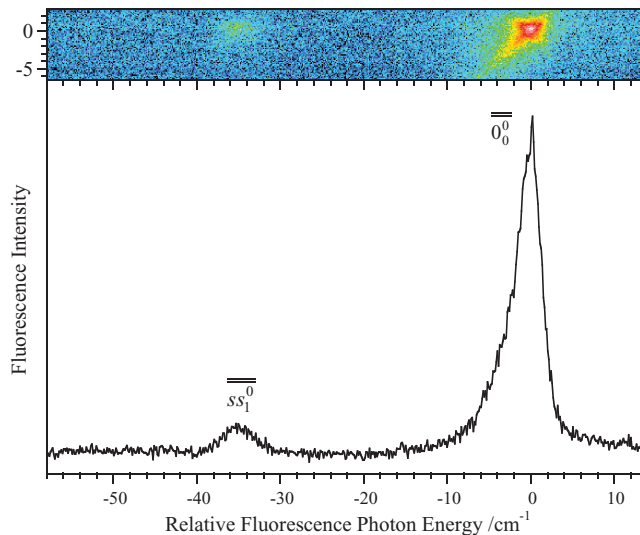


FIG. 5. The 2D-LIF image and corresponding dispersed fluorescence spectrum arising from scanning the laser over the $\overline{0}_0^0$ band of FB-Ar₂ and monitoring dispersed fluorescence in the region near $\overline{0}_0^0$. The image is displayed with the laser wavenumber on the vertical axis and dispersed fluorescence wavenumber along the horizontal axis. The dispersed fluorescence spectrum is extracted by integrating the image along the laser wavenumber axis.

the FB-Ar₂ $\overline{0}_0^0$ dispersed fluorescence spectrum extracted by integration along the laser axis.

The spectrum shows several distinct differences compared with the analogous FB-Ar spectrum (cf. Fig. 3). First, the spectrum only shows a single feature in addition to the $\overline{0}_0^0$ band. This feature is located at a displacement of 35.0 cm^{-1} from the $\overline{0}_0^0$ band. Interestingly, the band has a subtly different shape to the $\overline{0}_0^0$ band, being more symmetric compared with the sharper high energy edge seen for $\overline{0}_0^0$. The second major difference is that the relative intensity of this feature (compared with the $\overline{0}_0^0$ band intensity) is significantly higher (by a factor of ~ 3) compared with the brightest feature in the analogous FB-Ar van der Waals spectrum, which is assigned to the stretch fundamental. The band observed is assigned to the symmetric stretch fundamental. The rationale for the assignment is discussed in Sec. IV D.

The scan provides sufficient signal to enable us to extract a reasonable LIF contour for the $\overline{0}_0^0$ absorption. The contour obtained is presented and discussed in Sec. IV B.

IV. DISCUSSION

A. FB-Ar S_1 rotational constants and geometry

The rotational constants for the $\overline{0}_0^0$ level of FB-Ar were reported by Ford and Müller-Dethlefs as part of a ZEKE photoelectron spectroscopic study.²² However, subsequent CCSD(T) level *ab initio* calculations performed on this system by Fajín *et al.* predict a different set of constants.⁴ In particular, the C constant determined from the *ab initio* calculations is substantially smaller (by 10%) than that extracted from the fit to Ford and Müller-Dethlefs’ contour. Fajín *et al.*

reported that this difference is largely associated with the van der Waals bond length, and they noted that the experimental rotational constants imply a bond length of $3.33 \pm 0.11 \text{ \AA}$ compared with 3.527 \AA determined in the calculations. As a consequence of this discrepancy, Fajín *et al.* suggested that a re-examination of the rotational constants is required.

As discussed in Sec. III E, we have determined a new set of rotational constants for 0^0 FB-Ar by fitting the rotational contour of the 0^0 band. Our constants are slightly larger than those of Fajín *et al.* (see Table II), with differences of 0.5% for *A*, 2.4% for *B*, and 2.3% for *C*. Part of this small discrepancy is likely to arise from inaccuracies in the structure of FB itself. Fajín *et al.* undertook their FB-Ar calculations with a fixed, *ab initio*-determined S_1 FB structure that is reasonably poor at reproducing the rotational constants determined experimentally.¹³ Their FB geometry implies an *A* constant, for example, that is over 3% too large. Our new constants for FB-Ar are consistently smaller than the values reported by Ford and Müller-Dethlefs.²² As anticipated by Fajín *et al.*, the most significant difference occurs for the *C* constant, which Ford and Müller-Dethlefs found to be 7.2% larger than our value. The differences between our values and those of Ford and Müller-Dethlefs for the remaining constants are smaller at 0.7% and 0.8% for *A* and *B*, respectively. As discussed earlier, we ascribe the differences between our constants and those obtained by Ford and Müller-Dethlefs to saturation effects in the latter's spectrum.

In this context we note that Kalkman *et al.*³⁰ recently reported a high resolution study of the phenol-Ar dimer in which they were able to see detailed structure and determine accurate rotational constants. They found that the rotational constants determined were up to 4% different from those determined earlier by a fit to the rotational contour³¹ and suggested that this was illustrative of the limitations of such fits. However, examination of the earlier fit shows that it was less than ideal and, similar to the case for FB-Ar, the experimental rotational contour was measured using REMPI. We suggest that a fit to the rotational contour can provide significantly more accurate rotational constants than the phenol comparison indicates but, because the fit is sensitive to the intensity profile of the contour, one must be careful to ensure that the experimental contour is not compromised.

The experimental rotational constants can be used to extract the position of the Ar atom relative to the FB frame. If the geometry of the FB monomer is unchanged on complexation with Ar, there are only two additional geometric parameters in the FB-Ar complex. These are *R*, the distance from the Ar atom to the centre of mass of FB, and θ , the angle between the normal to the FB plane and the line joining the FB centre of mass to the Ar atom (the argon atom is constrained to lie within the FB out-of-plane mirror plane, thus restricting FB-Ar geometries to C_s symmetry). There are two approaches that can be taken to determine the argon position. First, if the geometry of FB is known, then *R* and θ can be determined from the rotational constants of FB-Ar. This is the approach taken by Stahl and Grabow in their study of S_0 FB-Ar.⁷ In that case the FB geometry determined by Doraiswamy and Sharma³² was used as the basis for determining the FB-Ar

geometry. Unfortunately, in the case of S_1 FB the experimental geometry is unknown so, instead, we use the result of *ab initio* calculations to determine the complex geometry using this approach. The second method available to determine the argon location is to derive relationships between the principal moments of inertia for the monomer and complex. Klots *et al.* and Spycher *et al.* have considered this case and provide relationships that express the moments of inertia for the complex in terms of those of the monomer and *R* and θ , obviating the need to know the FB geometry.^{33,34} S_1 FB rotational constants have recently been determined¹³ and thus the principal moments of inertia for the monomer and complex are known and can be used to locate the argon position.

As we have noted, the geometry of 0^0 FB has not been determined experimentally; however, recent *ab initio* calculations³⁵ have produced geometries that give rotational constants that are within 1% or better of the experimental FB constants.¹³ We have used the best *ab initio* geometry, as determined by the best match with the experimental FB rotational constants, as the basis for a calculation of the FB-Ar geometry, and hence rotational constants. The best FB geometry is provided by the CCSD(T) level calculations by Pugliesi and co-workers.^{13,35} The FB geometry was held at the *ab initio* value, while the Ar position was varied to provide the best match between the experimental and calculated FB-Ar rotational constants. The variation was confined to the plane perpendicular to the plane of the aromatic ring and incorporating the C-F bond (that is, C_s symmetry was preserved). The position that gave the best match with the experimental rotational constants is shown in Table III. In the absence of data from isotopically substituted species, experiment is unable to differentiate between the Ar being displaced from the FB CoM towards or away from the C-F bond. Isotopic substitution experiments⁸ and *ab initio* calculations^{2,3} have established that the Ar is displaced from the FB CoM towards the centre of the ring in S_0 . *Ab initio* calculations show that the displacement is also in this direction in S_1 .⁴

As stated above, the location of the argon atom in FB-Ar can also be estimated by exploiting relationships between the monomer and complex moments of inertia as discussed by Klots *et al.* and Spycher *et al.*^{33,34} Interestingly, the work of these authors revealed a need to adjust the effective moments of inertia for the monomer (FB in our case) to account for changes in the vibrationally averaged structure within the complex.^{33,34} They found it necessary to explicitly incorporate the effect of the large amplitude bending motions on the moments of inertia to account for deviations in the planar moments of inertia of the monomer and complex. We label the principal axes *x*, *y*, and *z*, where in the monomer we define the *x* axis to be along the C_2 axis, *y* perpendicular to it in the plane, and *z* out of the plane. In the case of FB-Ar, the *y* axis has the same direction as the monomer; however, the *x* and *z* principal axes are rotated slightly within the mirror plane. The planar moment of inertia, P_y , defined as

$$P_y = (I_z + I_x - I_y)/2,$$

should be the same for the complex and monomer, since only the atoms of the monomer have non-zero displacements from the *xz* plane.³³ However, this was not observed to be the case

TABLE III. The FB-Ar geometry calculated using various methods. R is the distance from the FB centre of mass (CoM) to the Ar atom; θ is the angle between the normal to the plane of the FB molecule and the line joining the Ar atom and the FB CoM; θ lies in the mirror plane of the complex. α is the average libration/rocking angle associated with zero point motion of the FB molecule within the complex (see text).

		R (Å)	θ (deg.)	α (deg.)	
S ₀ FB-Ar	Stahl and Grabow ^a	3.583	7.38	...	
	Our analysis: No correction ^b	3.585	7.12	...	
	Our analysis: Klots correction ^c	3.584	6.38	6.66	
	Our analysis: Spycher correction ^d	3.584	4.75	9.92	
	Fajin <i>et al.</i> (CCSD(T)) ^e	3.638	8.63	...	
	Makarewicz ^f (MP2/ADZ refined)	3.598	6.48	...	
	Makarewicz ^f (MP2/ADZ)	3.624	6.07	...	
	Makarewicz ^f (MP2/ADZ(-d,-2p))	3.631	6.05	...	
	S ₁ FB-Ar	Ford and Müller-Dethlefs ^g	3.42	13.2	...
		This work: From FB <i>ab initio</i> geometry ^h	3.481	7.06	...
This work: No correction ^b		3.489	6.60	...	
This work: Klots correction ^c		3.488	6.05	5.78	
This work: Spycher correction ^d		3.488	5.01	8.40	
Fajin <i>et al.</i> (CCSD(T)) ⁱ		3.540	4.99	...	

^aReference 7.

^bThe term “No correction” refers to the moments of inertia for the monomer retaining the same values in the complex.

^cThe moments of inertia for the monomer are corrected to account for bending motion in the complex using the method of Klots *et al.* (Ref. 33).

^dThe moments of inertia for the monomer are corrected to account for bending motion in the complex using the method of Spycher *et al.* (Ref. 34).

^eReference 2.

^fReference 3.

^gReference 22.

^hReferences 13 and 35.

ⁱReference 4.

for pyridine-Ar_{0,1,2} or furan-Ar_{0,1,2} comparisons.^{33,34,36} For pyridine-Ar, P_y is 0.8% smaller than P_y for pyridine, while for furan-Ar the reduction is 1.1%. In our case, P_y for FB-Ar is 1.5% smaller than that for FB. In the context of the earlier discussion concerning the accuracy of Ford and Müller-Dethlefs’ rotational constants for FB-Ar, it is interesting to note that their constants give a P_y for FB-Ar that is 15% different to that for FB. This large difference is further evidence that their set of FB-Ar constants is in error. Indeed, the consistency of the planar moments of inertia for the monomer and complex provides an indication of the reliability of the constants.

Klots *et al.* and Spycher *et al.* ascribe the small difference between the planar moments of inertia for the monomer and complex to the rocking motion of the planar molecule (associated with the van der Waals bends) effectively altering the vibrationally averaged distances to the atoms, and hence vibrationally averaged moments of inertia.^{33,34,36} To account

for this, the moments of inertia for the monomer must be replaced by “vibrationally averaged,” effective values when it is in the complex. From here on the term “effective moment of inertia,” I^{eff} , will be used to describe the vibrationally averaged moments of inertia associated with the monomer in the complex.

Klots *et al.*³³ and Spycher *et al.*³⁴ give different expressions for I^{eff} . The expressions relate I^{eff} of the monomer to the vibrationally averaged tilt angle of the ring, α . Spycher’s expressions are as follows:

$$I_x^{eff\text{FB}} = I_x^{\text{FB}} \left\langle 1 + \frac{1}{2} \sin^2 \alpha \right\rangle - P_z^{\text{FB}} \langle \sin^2 \alpha \rangle - \frac{1}{2} (I_x^{\text{FB}} - I_y^{\text{FB}}) \langle \sin^2 \alpha + \sin^4(\alpha/2) \rangle, \quad (1a)$$

$$I_y^{eff\text{FB}} = I_y^{\text{FB}} \left\langle 1 + \frac{1}{2} \sin^2 \alpha \right\rangle - P_z^{\text{FB}} \langle \sin^2 \alpha \rangle + \frac{1}{2} (I_x^{\text{FB}} - I_y^{\text{FB}}) \langle \sin^2 \alpha + \sin^4(\alpha/2) \rangle, \quad (1b)$$

$$I_z^{eff\text{FB}} = I_z^{\text{FB}} \left\langle 1 - \frac{1}{2} \sin^2 \alpha \right\rangle + P_z^{\text{FB}} \langle \sin^2 \alpha \rangle. \quad (1c)$$

The corresponding expressions of Klots *et al.* only involve the leading term in each of those above, for example, $I_x^{eff\text{FB}} = I_x^{\text{FB}} \langle 1 + \frac{1}{2} \sin^2 \alpha \rangle$. These equations involve vibrationally averaged expressions containing α , with the terms contained within $\langle \rangle$ indicating expectation values. Since α is small, $\sin \alpha \approx \alpha$ (α in radians) and the expectation values in the equations above can be expressed in terms of α^2 . For simplicity, in the discussion below we use α to indicate the root-mean-squared value.

The moments of inertia for the FB-Ar complex are given in terms of I^{eff} , R and θ ,³⁴

$$I_x^{\text{FB-Ar}} = \frac{1}{2} (I_x^{eff\text{FB}} + I_z^{eff\text{FB}} + \mu R^2) + \frac{1}{2} (I_x^{eff\text{FB}} - I_z^{eff\text{FB}} + \mu R^2 \cos 2\theta) \times (1 + \tan^2 2\gamma)^{1/2}, \quad (2a)$$

$$I_y^{\text{FB-Ar}} = I_y^{eff\text{FB}} + \mu R^2, \quad (2b)$$

$$I_z^{\text{FB-Ar}} = \frac{1}{2} (I_x^{eff\text{FB}} + I_z^{eff\text{FB}} + \mu R^2) - \frac{1}{2} (I_x^{eff\text{FB}} - I_z^{eff\text{FB}} + \mu R^2 \cos 2\theta) \times (1 + \tan^2 2\gamma)^{1/2}, \quad (2c)$$

where

$$\mu = \frac{m_{\text{Ar}} m_{\text{FB}}}{m_{\text{Ar}} + m_{\text{FB}}}$$

(m denotes the mass) and γ is the angle between the principal moments of inertia in the z direction for FB and FB-Ar. Furthermore, $\tan 2\gamma$ can be shown to be given by

$$\tan 2\gamma = \frac{2\mu R^2 \cos \theta \sin \theta}{I_z^{eff\text{FB}} - I_x^{eff\text{FB}} - \mu R^2 \cos 2\theta}.$$

While both Klots *et al.* and Spycher *et al.* determined the values for α , R , and θ via a global fit, we have chosen to do the fitting sequentially and first determine the value of α that

produces a set of I^{eff} (Eqs. (1) and (2)) such that the P_y calculated for the monomer using I^{eff} matches that experimentally determined for the complex. This was done by simply minimising the square of the difference between the observed P_y for the complex and the P_y calculated from I^{eff} , with α as the variable in the equations above. To confirm the validity of this approach we re-analysed the data of both Klots *et al.* and Spycher *et al.* and obtained the same values that they reported. With the value of α now fixed, the structural parameters R and θ can be determined by fitting the FB-Ar moments of inertia given by the expressions above to the experimental values. We have done this for both S_0 and S_1 by minimising the sum of the squares of the fractional differences between the calculated and observed values. Both the S_0 and S_1 FB-Ar geometries determined are given in Table III.

In the case of S_0 we have determined the Ar position using Stahl and Grabow's rotational constants for FB-Ar (Ref. 7) and the rotational constants for FB determined by Kisiel *et al.*³⁷ The S_0 FB-Ar geometry determined by Stahl and Grabow based on the FB geometry determined by Doraiswamy and Sharma is included in Table III for comparison. These results are compared with the geometries determined by recent *ab initio* calculations (accounting for zero-point motion) for the complex. It can be seen from Table III that the correction for effective moments of inertia makes only small differences to the value for R determined. However, the value for θ is significantly influenced by this correction, varying between 4.75° and 7.12° . The need to introduce the α -based correction to the moments of inertia indicates that the position of the Ar atom is not well localised as a result of the large amplitude bending motion. Thus, this variation in θ with different approaches is not surprising. The value of θ is largest with no correction to the FB moments of inertia and is smallest using the Spycher correction. The corrections effectively reduce the value of θ by adding the extra angular term, α . With α neglected, θ is largest. The Spycher correction gives the largest value of α and, as a consequence, the smallest value for θ . The geometry deduced by Stahl and Grabow from the FB geometry should be compared with the $\alpha = 0$ case, since it involves no adjustment of the FB geometry and hence moments of inertia within the complex. It can be seen that Stahl and Grabow determine a very slightly shorter R and slightly larger θ value compared with the geometry determined using the FB moments of inertia without correction, whereas they should give the same result if the FB geometry accurately reproduces the moments of inertia. The *ab initio* calculations predict a larger value for R than is determined from the experimental data. The CCSD(T) calculations are the furthest from the observed value. The MP2 approach used by Makarewicz gives values of θ within the range of those deduced from experiment while the CCSD(T) value is again larger than observed.

Turning now to the S_1 case, we see that as for S_0 there is little difference between the R values for the three methods of analysis, while the θ value decreases from the no correction case to the Spycher correction. The R values, as determined from experimental data, have decreased by 0.096 \AA from S_0 to S_1 . The range of θ values determined by the three approaches is narrower for the S_1 analysis, varying from 6.60°

to 5.01° . Given the ranges in both cases, it is difficult to be definitive concerning any change in this angle from S_0 to S_1 . The CCSD(T) calculations again predict a larger value for R than is determined from the experimental data. The difference in both the S_0 and S_1 cases is $\sim 0.05 \text{ \AA}$. The calculations predict a value for θ that is at the lower end of the range determined from the experimental data. The rotational constants determined by Ford and Müller-Dethlefs lead to an R value that is too small and a θ value that is too large. The FB-Ar geometry determined using the *ab initio* geometry for FB as a basis gives a value for R that is $< 0.1 \text{ \AA}$ and $\sim 1^\circ$ different from the geometry deduced from the experimental moments of inertia.

B. Predicted FB-Ar₂ rotational constants and comparison with the observed contour

There is significant evidence that a second Ar on the opposite face of an aromatic ring is negligibly influenced by the presence of the first.¹⁴⁻¹⁹ For example, the pyridine-Ar_{1,2} complexes give an R change of 0.0019 \AA and θ change of 0.61° (Ref. 34) while for furan-Ar_{1,2} the change in R is 0.0042 \AA with a θ change of 0.43° (Ref. 36). Interestingly, a recent analysis of phenol-Ar_{1,2} suggests a lengthening of the bond in the trimer by $\sim 0.02 \text{ \AA}$ compared to the dimer,³⁰ which is larger than that seen in the pyridine and furan systems. The positions that we have determined for the Ar atom in $\overline{0^0}$ and $\overline{0_0}$ FB-Ar are expected to be very similar for both Ar atoms in FB-Ar₂ (1|1), providing a means to predict rotational constants for $\overline{0^0}$ and $\overline{0_0}$ FB-Ar₂ (1|1), and hence a prediction to be made of the $\overline{0_0^0}$ band rotational contour for FB-Ar₂ (1|1).

In calculating the FB-Ar₂ (1|1) rotational constants it is necessary to assume that R and θ are the same in the FB-Ar and FB-Ar₂ complexes. Typical variations in R and θ have been given above. We need to consider the effect of changes to I^{eff} since, as the bend vibrations are different in the dimer and trimer complexes, the effective moments of inertia for FB need not be the same in the two complexes. This has been seen for the pairs pyridine-Ar_{1,2} (Ref. 34) and furan-Ar_{1,2} (Ref. 36). We have analysed the M-Rg_{0,1,2} systems pyridine-Ar_{0,1,2} (Ref. 34), furan-Ar_{0,1,2} (Ref. 36), pyridine-Ne_{0,1,2} (Ref. 38), and phenol-Ar_{0,1,2} (Refs. 30 and 39) to assess which method of determining I^{eff} , R and θ from analysis of the M-Rg_{0,1} rotational constants (see Sec. IV A) gives the most accurate prediction for the M-Rg₂ rotational constants. Expressions for the M-Rg₂ moments of inertia have been given by Spycher *et al.*³⁴ The results of the analysis are summarised in Table IV. Phenol has been assumed to be C_{2v} symmetry for the purposes of this comparison. The Klots and Spycher methods, which include correction to the monomer moments of inertia, are generally significantly better predictors of the trimer rotational constants. Interestingly, in all cases the Klots method leads to a more accurate prediction than the Spycher approach despite the latter's increased sophistication.

The predicted FB-Ar₂ (1|1) rotational constants, calculated using the three approaches to determining the I^{eff} , R and θ values, are given in Table V and the rotational contour calculated using these constants is shown in Fig. 6. The

TABLE IV. A comparison between the observed rotational constants for M-Rg₂ trimers and those predicted from the M-Rg geometry determined from the M and M-Rg rotational constants.

		Rotational constants ^a				% Differences			Figure of Merit ^b		
		Observed ^c	Calculated			No correction	Klots correction	Spycher correction	No correction	Klots correction	Spycher correction
			No correction ^d	Klots correction ^e	Spycher correction ^f						
Furan-Ar ₂	A	4187.7	3947.1	4205.2	4212.0	5.74	-0.42	-0.58	5.86	0.67	0.81
	B	493.81	499.02	491.78	491.60	-1.06	0.41	0.45			
	C	486.56	488.88	485.03	484.94	-0.48	0.32	0.33			
Pyridine-Ar ₂	A	2938.5	2849.1	2950.2	2955.2	3.04	-0.40	-0.57	3.15	0.46	0.64
	B	466.56	469.97	465.71	465.48	-0.73	0.18	0.23			
	C	464.14	465.65	463.46	463.35	-0.32	0.15	0.17			
Pyridine-Ne ₂	A	2957.4	2881.3	2970.9	2975.5	2.57	-0.46	-0.61	2.73	0.47	0.64
	B	931.54	939.39	930.61	930.01	-0.84	0.10	0.17			
	C	922.54	925.63	922.20	922.06	-0.33	0.04	0.05			
Phenol-Ar ₂	A	1777.6	1757.1	1778.9	1811.1	1.16	-0.07	-1.88	1.28	0.82	2.40
	B	462.5	460.67	459.57	456.45	0.40	0.63	1.31			
	C	420.7	419.11	418.55	417.69	0.38	0.51	0.71			

^aRotational constants are given in units of MHz.

^bThe figure of Merit is defined as the square root of the sum of the squares of the % differences for the three rotational constants.

^cObserved values are from Ref. 43 (furan-Ar₂), Ref. 34 (pyridine-Ar₂), Ref. 38 (pyridine-Ne₂), and Ref. 30 (phenol-Ar₂). With the exception of phenol-Ar₂, the observed values are typically reported to eight significant figures. They have been truncated to five significant figures here for clarity in comparing with the calculated values, which typically differ from the observed values in the third significant figure.

^dThe term "No correction" refers to the moments of inertia for the monomer retaining the same values in the complex.

^eThe moments of inertia for the monomer are corrected to account for bending motion in the complex using the method of Klots *et al.* (Ref. 33).

^fThe moments of inertia for the monomer are corrected to account for bending motion in the complex using the method of Spycher *et al.* (Ref. 34).

temperature used for calculating the contours was 4.4 K, the same as the FB-Ar value determined in the fit for that contour. Figure 6 also includes the experimentally observed 0_0^0 band rotational contour for FB-Ar₂ (1|1). The rotational contours are primarily sensitive to the differences between the rotational constants in the S₀ and S₁ states. We find that at the resolution of our experiment there is no discernible difference in the rotational contours calculated with the three sets of predicted rotational constants.

The comparison between the experimental and predicted contours is unexpectedly poor. Because high laser power had to be used to observe the contour, based on our FB-Ar mea-

surements we expect some saturation effects to be present, but the differences observed go well beyond what could be attributed to saturation. In particular, there is a "tail" at low energy in the experimental contour that is not reproduced by the calculated contour. Increasing the temperature causes the peak of the contour to broaden and the contour to extend to higher energy, so this does not explain the tail observed.

We have fitted the experimental contour to obtain an indication of the magnitude of the change in rotational constants between S₀ and S₁ required to explain its shape.

TABLE V. Predicted FB-Ar₂ rotational constants and the difference between the S₀ and S₁ constants (Δ). The constants are given in units of cm⁻¹.

		Rotational constant	No correction ^a	Klots correction ^b	Spycher correction ^c
S ₀ FB-Ar ₂	A		0.057246	0.057960	0.059053
	B		0.015318	0.015273	0.015164
	C		0.013857	0.013832	0.013803
S ₁ FB-Ar ₂	A		0.056083	0.056573	0.057243
	B		0.015986	0.015955	0.015879
	C		0.014458	0.014439	0.014420
$\Delta(S_0 - S_1)$	A		0.001163	0.001387	0.001810
	B		-0.000667	-0.000682	-0.000715
	C		-0.000601	-0.000608	-0.000617

^aThe term "No correction" refers to the moments of inertia for the monomer retaining the same values in the complex.

^bThe moments of inertia for the monomer are corrected to account for bending motion in the complex using the method of Klots *et al.* (Ref. 33).

^cThe moments of inertia for the monomer are corrected to account for bending motion in the complex using the method of Spycher *et al.* (Ref. 34).

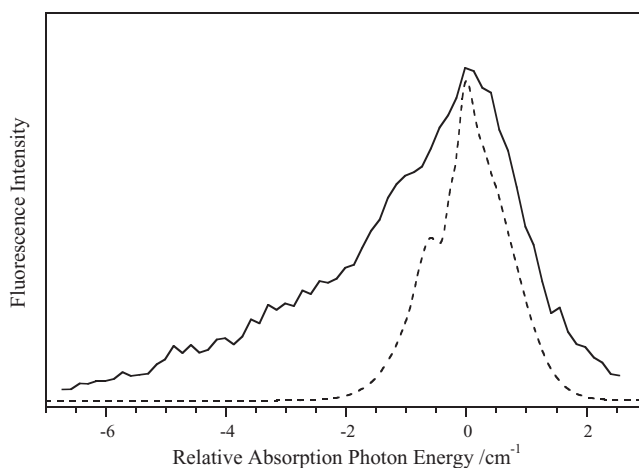


FIG. 6. The LIF contour for the FB-Ar₂ 0_0^0 band (solid line) extracted by vertically integrating a horizontal slice taken from Fig. 1(b). The predicted contour is also shown as a dashed line (see text). For the purpose of comparison, the peak positions of the two spectra have been aligned. The x axis represents the shift from the peak position. The rotational constants associated with the predicted contour are shown in Table V.

Using the calculated ground state values shown in Table V, we find that the excited state values required to reproduce the contour imply a FB-Ar bond length of $R = 5.9 \text{ \AA}$ (cf. 3.49 \AA in the dimer) which is clearly nonsensical. This analysis reveals that the contour cannot be due to FB-Ar₂ alone. We suggest that the observed contour includes an overlapping feature on the low energy side that is responsible for the tail. The FB-Ar₂ (1|1) contour warrants further investigation and would appear to be a system ripe for more detailed study.

C. van der Waals vibrational structure of FB-Ar

1. The S₀ vibrational states

Ab initio calculations have predicted the van der Waals vibrational structure for S₀ FB-Ar, at least in the lower part of the potential well.^{2,3} However, prior to the present work only the two bend fundamental frequencies had been reported for S₀ FB-Ar, giving limited data to test these predictions. This situation is typical, primarily because of the comparative complexity of the laser-based experimental methods that have characteristically been used to observe transitions to ground state van der Waals vibrations. A significant study in this regard is due to Maxton *et al.* who observed intermolecular vibrational modes in a series of aromatic-rare gas van der Waals complexes, including FB-Ar.¹² Their Raman technique is primarily sensitive to the bend motions and their FB-Ar spectrum revealed the long and short axis bend fundamentals, $\nu_{bl} = 22.5 \text{ cm}^{-1}$ and $\nu_{bs} = 33.5 \text{ cm}^{-1}$, respectively. No other S₀ van der Waals vibrations have previously been reported for FB-Ar.

There have been two reports of *ab initio* studies of the S₀ FB-Ar complex for which the van der Waals vibrational levels have been determined. Fajín *et al.* reported vibrational levels up to 75 cm^{-1} (Ref. 2), while the subsequent study by Makarewicz reported levels up to 70 cm^{-1} (Ref. 3). In both cases they largely compare their S₀ calculations with observed S₁ frequencies (with the exception of the two bend fundamentals noted above) because of the lack of experimental data. Fajín *et al.* noted that the availability of theoretical values could aid future assignments as data became available.

Our spectrum reveals five vibrational levels in the S₀ state up to an energy of 65 cm^{-1} , which is within the region covered by the two sets of calculations. The comparison between our observed bands and the *ab initio* calculations of Fajín *et al.* and Makarewicz are shown in Table VI. The agreement between the calculated and observed energies is quite impressive, with deviations less than 1 cm^{-1} . There is a trend for the calculations to lie slightly below the observed values. Unlike the S₁ case discussed below, relative intensities were not calculated for the $\bar{0}^0$ emission transitions.

2. The S₁ state

S₁ van der Waals vibrational features have been observed up to 66 cm^{-1} . These modes have been reported in previous mass-resolved REMPI studies and our work confirms, via the 2D-LIF rotational contours, these earlier assignments. As discussed in Sec. III E, the FB-Ar transitions are easily satu-

TABLE VI. A comparison between the experimentally observed S₀ vibrational levels and those calculated by *ab initio* methods.

Level number ^a	Assignment ^b	Energy (cm ⁻¹)			
		<i>Ab initio</i>		Experimental	
		Fajín <i>et al.</i> ^c	Makarewicz ^d	This work ^e	Maxton <i>et al.</i> ^f
0	(0, 0, 0)	0	0	0	0
1	(0, 1, 0)	22.0	21.9	22.3	22.5
2	(1, 0, 0)	33.2	33.4	33.6	33.5
3	(0, 2, 0)	37.1	37.6	37.6	
4	(0, 0, 1)	44.4	45.2	45.4	
8	(2, 0, 0)	64.6	65.4	65.0	

^aThe level numbering is the ordering given by Fajín *et al.* (Ref. 2).

^bAssignments are given in the form ($\nu_{\text{short bend}}$, $\nu_{\text{long bend}}$, ν_{stretch}). The assignments involving the Fermi resonance between (0, 2, 0) and (0, 0, 1) are labelled by their “zero-order” character.

^cCCSD(T) *ab initio* calculations (Ref. 2).

^dMP2 *ab initio* calculations (Ref. 3).

^eWhere a vibrational level has been determined multiple times, the average value is given.

^fReference 12.

rated, and indeed the LIF rotational contour of $\bar{0}^0$ presented in Fig. 2 does show some saturation effect when compared to that collected in the linear region (Fig. 4). Although the Q branch is attenuated in the extended scans, the integrated band intensity will only be slightly affected by this. In this context we note that all FB-Ar features in our spectra clearly show the strong Q branch yet this is not prominent in previously reported spectra. The *ab initio* calculations of Fajín *et al.* included predictions of both the van der Waals vibrational state energies and their relative intensities in transitions from $\bar{0}_0$.⁴ The shifts associated with van der Waals bands and their relative intensities are shown in Table VII. This table compares our work with both previous experimental data and *ab initio* calculation.

Comparing our experimental values to those obtained via *ab initio* methods, there are larger differences between experimental and *ab initio* energies in the S₁ level than we saw for S₀, with a difference of up to 2 cm^{-1} . Interestingly, the calculated and observed intensities show an excellent match with *ab initio* calculations, with the exception of the short axis bend fundamental and overtone. Since the transition dipole for the S₁ ← S₀ transition of FB lies in-plane perpendicular to the C–F bond,⁴⁰ the short axis bend of FB-Ar is forbidden by symmetry if the complex is viewed as C_s. This may be the origin of the difference. Our relative intensities for the van der Waals modes are generally lower than those reported by previous authors which is associated with the saturation issues discussed previously.

3. Fermi resonances

An interesting issue concerning the assignments of the van der Waals features is the extent to which the states are mixed through anharmonic interactions. Bieske *et al.* proposed that the stretch fundamental and bend overtones couple through a generic kinetic anharmonic mechanism and argued that this should be a ubiquitous feature of aromatic-rare-gas

TABLE VII. A comparison of the S_1 van der Waals vibrational levels observed and their relative intensities with those calculated. Previously reported experimental values are included.

Level number ^a	Assignment ^b	<i>Ab initio</i>		Experimental							
		Fajín <i>et al.</i> ^c		This work ^d		Grebner and Neusser ^e		Lembach and Brutschy ^f		Bieske <i>et al.</i> ^g	
		E (cm ⁻¹)	I _{rel}	E (cm ⁻¹)	I _{rel}	E (cm ⁻¹)	I _{rel}	E (cm ⁻¹)	I _{rel}	E (cm ⁻¹)	I _{rel}
0	(0,0,0)	0	100	0	100	0	100	0	...	0	100
1	(0,1,0)	20.17	0.5	19.7	0.44	20	1.7	20	...	21	7
2	(1,0,0)	30.94	0.4	32.2	1.3	32	2.0			34	7
3	(0,2,0)	36.16	1.3	35.3	1.3	35	2.5			38	12
4	(0,0,1)	44.12	4.9	43.5	4.8	44	12	43	...	47	22
6	(0,3,0)	51.33	0.1							54	1
7	(2,0,0)	61.55	1.0	63.5	0.62	64	2.0			70	3
8	(0,4,0)/(0,1,1)	62.13	0.2								

^aThe level numbering is that introduced by Fajín *et al.* (Ref. 4).

^bAssignments are those given by Fajín *et al.* (Ref. 4) and are in the form ($\nu_{\text{short bend}}, \nu_{\text{long bend}}, \nu_{\text{stretch}}$). The assignments involving the Fermi resonance between (0, 2, 0) and (0, 0, 1) are labelled by their “zero-order” character.

^cReference 4.

^dIntensities given for this work are for the ($\nu dW_0^n, \nu dW_n^n$) 2D-LIF transition.

^eReference 6.

^fReference 5.

^gReference 9.

complexes.⁹ In their model the authors proposed a three level interaction involving the stretch coupling to each of the two bend overtones. This has since been shown to be incorrect as the short axis bend fundamental was wrongly assigned as the overtone.² Nevertheless, the proposition that the stretch and long axis bend overtone interact anharmonically has merit. The vibrational wavefunctions determined by the *ab initio* calculations reported in Refs. 2–4 are based on the calculated potential energy surface, and thus intrinsically account for such coupling. It was found for both S_0 and S_1 that the displacements of the Ar atom for the bend overtone and stretch are not simple bending and stretching motions but are mixtures of both, consistent with the proposed coupling mechanism.^{2–4}

Data from the 2D-LIF spectral images provide a means to test the extent to which the spectra can be explained in terms of a cubic anharmonic coupling between the stretch and two quanta of the long axis bend. The wavefunctions for the two molecular states can be expressed as linear combinations of the long axis bend overtone, $|\phi_{2bl}\rangle$, and stretch states, $|\phi_s\rangle$,

$$|\psi_{upper}\rangle = c_1 |\phi_s\rangle + c_2 |\phi_{2bl}\rangle \text{ and}$$

$$|\psi_{lower}\rangle = -c_2 |\phi_s\rangle + c_1 |\phi_{2bl}\rangle.$$

The usual starting point is to assume that only one of the zero-order states carries oscillator strength. In the present case, for absorption transitions from $\overline{0_0}$ or fluorescence transitions from $\overline{0^0}$ this is the stretch since the similar frequencies for the bend in S_0 and S_1 lead to the expectation that the Franck Condon factors for the $\Delta\nu = 2$ transition will be significantly smaller than the $\Delta\nu = 1$ transition of the stretch. With this approximation, a spectrum can be analysed to yield the separation between the zero-order states $|\phi_{2bl}\rangle$ and $|\phi_s\rangle$, the coupling constant, V , and the coefficients, c_1 and c_2 .

Since the long axis bend overtone is seen in both absorption from $\overline{0_0}$ and emission from $\overline{0^0}$, the resonance appears

to be present in both S_0 and S_1 . Deconvoluting the spectra we find that for S_1 the zero-order states are separated by 4.8 cm⁻¹ and V is 2.6 cm⁻¹. As a consequence of this relatively large separation compared with the coupling strength, the resulting molecular states are moderately mixed. The molecular states are $|\psi_{upper}\rangle = 0.89|\phi_s\rangle + 0.45|\phi_{2bl}\rangle$ and $|\psi_{lower}\rangle = -0.45|\phi_s\rangle + 0.89|\phi_{2bl}\rangle$. We find the states to be significantly more mixed in S_0 , where the zero-order states are separated by 1.5 cm⁻¹ and V is 3.8 cm⁻¹. The resulting molecular states in S_0 are $|\psi_{upper}\rangle = 0.77|\phi_s\rangle + 0.64|\phi_{2bl}\rangle$ and $|\psi_{lower}\rangle = -0.64|\phi_s\rangle + 0.77|\phi_{2bl}\rangle$.

A test for this model is the extent to which it accurately predicts spectra from other levels. In particular, do the molecular states determined allow one to accurately predict the relative intensities of transitions between them? This can be tested since in the 2D-LIF spectral images in Fig. 1 we observe fluorescence transitions from the mixed states in S_1 to those in S_0 . It is straightforward to calculate what the relative intensities should be in these spectra from the molecular state coefficients determined above. In principal, fluorescence from the “stretch” should terminate in the “bend overtone” and the “stretch” in the same ratio as fluorescence from the “bend overtone” terminates in the “stretch” and “bend overtone.” That is, the intensity ratio between the features ($\overline{s_0^1}, \overline{s_0^1 bl_2^0}$) and ($\overline{s_0^1}, \overline{s_1^1}$) should be equal to the ratio between ($\overline{bl_0^2}, \overline{bl_0^2 s_1^0}$) and ($\overline{bl_0^2}, \overline{bl_2^2}$). Based on the coefficients calculated above this ratio is expected to be 4.9%. The observed values are $7.5 \pm 0.9\%$ and $5.8 \pm 2.3\%$, respectively, which is in reasonable agreement. We conclude that the spectra can be well described in terms of a cubic anharmonic coupling between the stretch and long axis bend overtone.

It is interesting in this context to compare the wavefunctions that we calculate with those determined in the *ab initio* calculations. While this comparison can only be qualitative, it is nevertheless instructive. From the displacements reported for the calculated long axis bend overtone and stretch

wavefunctions,^{2,3} it is clear that the wavefunctions are very similar in S_0 , consistent with our analysis. Furthermore, the S_1 wavefunctions are much more distinct,⁴ again consistent with our results.

D. The FB-Ar₂ (1|1) van der Waals vibrations

There are few examples of spectra revealing the intermolecular vibrations of aromatic-Rg₂ (Rg = rare gas) (1|1) trimers. Bieske, Rainbird, and Knight reported mass-resolved REMPI spectra that revealed the S_1 van der Waals modes of aniline-Ar₂.⁴¹ Given that the second Ar occupies an equivalent position to the first, the authors related the observed vibrational energies to those of the aniline-Ar dimer. Subsequently, Maxton *et al.* observed intermolecular bend vibrations for the related dimer and trimer species benzene-Ar_{1,2} and fluorene-Ar_{1,2}.¹² Like Bieske *et al.*, they presented a framework for determining intermolecular vibrational frequencies for the trimer, although their considerations were restricted to the modes expected to show Raman activity. Their Raman technique is primarily sensitive to the intermolecular bend modes involving libration of the aromatic. Phenol-Ar₂ provides a recent example where the S_1 vibrational structure of an aromatic-Rg₂ trimer has been observed,⁴² although in that case it was a precursor to a more detailed study of the intermolecular modes of the corresponding cation.

As discussed in Sec. III F, dispersed fluorescence from the $\overline{00}$ level of FB-Ar₂ (1|1) reveals a feature at 35.0 cm⁻¹ associated with an S_0 van der Waals vibration (see Fig. 5). The formulas provided by Bieske *et al.* allow the six FB-Ar₂ (1|1) intermolecular vibrational frequencies to be calculated from the three FB-Ar intermolecular frequencies and various constants associated with the complex.⁴¹ Based on the intensities seen in the dimer, the symmetric stretch is expected to be the most intense band observed in the trimer. Its expected frequency in terms of the FB-Ar dimer stretch frequency is

$$\nu_{\text{trimer}} = \nu_{\text{dimer}} \sqrt{\frac{\mu_{\text{dimer}}}{\mu_{\text{trimer}}}},$$

where ν_{dimer} is the stretch frequency in the dimer and μ_{dimer} and μ_{trimer} are the reduced masses for the dimer stretch and trimer symmetric stretch, respectively,

$$\mu_{\text{dimer}} = \left(\frac{1}{m_{\text{Ar}}} + \frac{1}{m_{\text{FB}}} \right)^{-1}; \mu_{\text{trimer}} = m_{\text{Ar}},$$

where m_{Ar} denotes the mass of Ar and m_{FB} denotes the mass of FB.

Using a FB-Ar stretch frequency of 42.5 cm⁻¹, the value is that obtained by de-perturbing the Fermi resonance, we obtain a FB-Ar₂ (1|1) symmetric stretch frequency of $\nu_{\text{ss}} = 35.7$ cm⁻¹, in good agreement with the 35.0 cm⁻¹ of the observed band. It is interesting to note that the agreement is less satisfactory if the observed FB-Ar stretch value of 45.4 cm⁻¹ is used rather than the de-perturbed value. In this case the predicted ν_{ss} value is 38.2 cm⁻¹, some 3.2 cm⁻¹ higher than the observed value.

V. CONCLUSIONS

We have used the technique of 2D-LIF spectroscopy to explore the van der Waals complexes fluorobenzene-Ar and fluorobenzene-Ar₂ in the region of their S_1 - S_0 electronic origins. The features due to the monomer and each of the complexes are readily discerned in the 2D-LIF spectral images due to their different shapes. Features associated with the fluorobenzene-Ar complex in particular are readily recognized by the presence of a sharp Q branch. The images reveal features associated with the van der Waals vibrations in S_0 and S_1 . The use of 2D-LIF spectroscopy to extract the LIF spectrum associated with a particular species was illustrated by extracting the LIF spectrum for fluorobenzene-Ar from an appropriate slice of the image. The S_1 van der Waals modes observed in this spectrum are consistent with previous observations using mass resolved REMPI techniques. Dispersed fluorescence spectra associated with particular absorption features are also readily extracted, allowing the observation of van der Waals vibrations in the ground electronic state.

The fluorobenzene-Ar $\overline{00}$ rotational contour has been analysed to yield a set of S_1 rotational constants $A' = 0.05871 \pm 0.00014$ cm⁻¹, $B' = 0.03803 \pm 0.00010$ cm⁻¹, and $C' = 0.03103 \pm 0.00003$ cm⁻¹. These constants imply that in S_1 the Ar is 3.488 Å from the fluorobenzene centre of mass and displaced from it towards the centre of the ring at an angle of $\sim 6^\circ$ to the normal. It should be noted that these values refer to the expectation values in the S_1 zero point vibrational level and, given that the complex is “floppy,” the Ar atom will be undergoing significant motion about these values. The rotational contour for fluorobenzene-Ar₂ has been predicted using rotational constants calculated on the basis of the fluorobenzene-Ar geometry and compared with the experimental contour. The comparison is poor and suggests the presence of another band lying beneath the low energy edge of the contour.

The 2D-LIF spectral images reveal van der Waals vibrational modes in both S_0 and S_1 up to 65 cm⁻¹. Comparisons with the results of *ab initio* calculations show excellent agreement, although there is a trend for the calculated values to generally be slightly lower than those observed. There is good agreement overall with the calculated relative intensities for excitation of van der Waals modes in the LIF spectrum, although there are clear differences associated with the short axis bend. The Fermi resonance between the stretch and bend overtone has been analysed in both the S_0 and S_1 states. The analysis reveals that the coupling is stronger in S_0 than in S_1 and the resulting mixed wavefunctions are qualitatively consistent with the *ab initio* results.

The 2D-LIF image reveals the S_0 symmetric stretch van der Waals vibration in fluorobenzene-Ar₂ to be at 35.0 cm⁻¹. The observed value closely matches that predicted based on the fluorobenzene-Ar van der Waals stretch frequency.

ACKNOWLEDGMENTS

We thank Aaron Hunter for his help in collecting the laser power dependence data required to confirm that the fluorobenzene-Ar rotational contour was collected in

the region of linear dependence. We also thank Timothy Solheim for preliminary analysis of the fluorobenzene-Ar₂ rotational contour. We acknowledge and thank Colin Western for providing a Command line version of his PGOPHER program and Dr. Martin Cockett from the University of York for supplying fluorobenzene geometries from his group's *ab initio* calculations. We thank the School's Electronic and Mechanical workshop staff for their support in constructing and maintaining the apparatus. This research was supported by the Australian Research Council and Flinders University.

- ¹K. S. Kim, P. Tarakeshwar, and J. Y. Lee, *Chem. Rev.* **100**, 4145 (2000).
- ²J. L. C. Fajín, J. L. Cacheiro, B. Fernandez, and J. Makarewicz, *J. Chem. Phys.* **120**, 8582 (2004).
- ³J. Makarewicz, *J. Chem. Phys.* **121**, 8755 (2004).
- ⁴J. L. C. Fajín, S. B. Capelo, B. Fernandez, and P. M. Felker, *J. Phys. Chem. A* **111**, 7876 (2007).
- ⁵G. Lembach and B. Brutschy, *J. Phys. Chem.* **100**, 19758 (1996).
- ⁶T. L. Grebner and H. J. Neusser, *Int. J. Mass Spectrom. Ion Process.* **159**, 137 (1996).
- ⁷W. Stahl and J. U. Grabow, *Z. Naturforsch.* **47a**, 681 (1992).
- ⁸R. A. Appleman, S. A. Peebles, and R. L. Kuczkowski, *J. Mol. Struct.* **446**, 55 (1998).
- ⁹E. J. Bieske, M. W. Rainbird, I. M. Atkinson, and A. E. W. Knight, *J. Chem. Phys.* **91**, 752 (1989).
- ¹⁰G. Lembach and B. Brutschy, *J. Chem. Phys.* **107**, 6156 (1997).
- ¹¹H. Shinohara, S. Sato, and K. Kimura, *J. Phys. Chem. A* **101**, 6736 (1997).
- ¹²P. M. Maxton, M. W. Schaeffer, S. M. Ohline, W. Kim, V. A. Ventura, and P. M. Felker, *J. Chem. Phys.* **101**, 8391 (1994).
- ¹³J. R. Gascooke, U. N. Alexander, and W. D. Lawrance, *J. Chem. Phys.* **134**, 184301 (2011).
- ¹⁴C. A. Haynam, D. V. Brumbaugh, and D. H. Levy, *J. Chem. Phys.* **80**, 2256 (1984).
- ¹⁵J. C. Alfano, S. J. Martinez, and D. H. Levy, *J. Chem. Phys.* **94**, 1673 (1991).
- ¹⁶T. Weber and H. J. Neusser, *J. Chem. Phys.* **94**, 7689 (1991).
- ¹⁷R. Sussmann and H. J. Neusser, *Chem. Phys. Lett.* **221**, 46 (1994).
- ¹⁸R. Sussmann, U. Zitt, and H. J. Neusser, *J. Chem. Phys.* **101**, 9257 (1994).
- ¹⁹S. M. Bellm and W. D. Lawrance, *Chem. Phys. Lett.* **368**, 542 (2003).
- ²⁰N. Gonohe, A. Shimizu, H. Abe, N. Mikami, and M. Ito, *Chem. Phys. Lett.* **107**, 22 (1984).
- ²¹N. Gonohe, H. Abe, N. Mikami, and M. Ito, *J. Phys. Chem.* **89**, 3642 (1985).
- ²²M. S. Ford and K. Müller-Dethlefs, *Phys. Chem. Chem. Phys.* **6**, 23 (2004).
- ²³K. Rademann, B. Brutschy, and H. Baumgärtel, *Chem. Phys.* **80**, 129 (1983).
- ²⁴P. Hobza, H. L. Selzle, and E. W. Schlag, *J. Chem. Phys.* **99**, 2809 (1993).
- ²⁵P. Tarakeshwar, K. S. Kim, E. Kraka, and D. Cremer, *J. Chem. Phys.* **115**, 6018 (2001).
- ²⁶E. D. Lipp and C. J. Seliskar, *J. Mol. Spectrosc.* **87**, 255 (1981).
- ²⁷R. Vasudev and J. C. D. Brand, *J. Mol. Spectrosc.* **75**, 288 (1979).
- ²⁸E. D. Lipp and C. J. Seliskar, *J. Mol. Spectrosc.* **87**, 242 (1981).
- ²⁹C. M. Western, pgopher, a Program for Simulating Rotational Structure, University of Bristol; see <http://pgopher.chm.bris.ac.uk>.
- ³⁰I. Kalkman, C. Brand, T. B. C. Vu, W. L. Meerts, Y. N. Svartsov, O. Dopfer, X. Tong, K. Müller-Dethlefs, S. Grimme, and M. Schmitt, *J. Chem. Phys.* **130**, 224303 (2009).
- ³¹M. S. Ford, S. R. Haines, I. Pugliesi, C. E. H. Dessent, and K. Müller-Dethlefs, *J. Electron Spectrosc. Relat. Phenom.* **112**, 231 (2000).
- ³²S. Doraiswamy and S. D. Sharma, *J. Mol. Struct.* **102**, 81 (1983).
- ³³T. D. Klots, T. Emilsson, R. S. Ruoff, and H. S. Gutowsky, *J. Phys. Chem.* **93**, 1255 (1989).
- ³⁴R. M. Spycher, D. Petitprez, F. L. Bettens, and A. Bauder, *J. Phys. Chem.* **98**, 11863 (1994).
- ³⁵I. Pugliesi, N. M. Tonge, and M. C. R. Cockett, *J. Chem. Phys.* **129**, 104303 (2008).
- ³⁶R. M. Spycher, L. Hausherr-Primo, G. Grassi, and A. Bauder, *J. Mol. Struct.* **351**, 7 (1995).
- ³⁷Z. Kisiel, E. Bialkowska-Jaworska, and L. Pszczolkowski, *J. Mol. Spectrosc.* **232**, 47 (2005).
- ³⁸L. Evangelisti, L. B. Favero, B. M. Giuliano, S. Y. Tang, S. Melandri, and W. Caminati, *J. Phys. Chem. A* **113**, 14227 (2009).
- ³⁹G. Berden, W. L. Meerts, M. Schmitt, and K. Kleinermanns, *J. Chem. Phys.* **104**, 972 (1996).
- ⁴⁰G. H. Kirby, *Mol. Phys.* **19**, 289 (1970).
- ⁴¹E. J. Bieske, M. W. Rainbird, and A. E. W. Knight, *J. Chem. Phys.* **94**, 7019 (1991).
- ⁴²A. Armentano, X. Tong, M. Riese, S. M. Pimblott, K. Müller-Dethlefs, M. Fujii, and O. Dopfer, *Phys. Chem. Chem. Phys.* **13**, 6071 (2011).
- ⁴³R. M. Spycher, P. M. King, and A. Bauder, *Chem. Phys. Lett.* **191**, 102 (1992).